Nuclear Inst. and Methods in Physics Research, A 972 (2020) 164122

Contents lists available at ScienceDirect

Nuclear Inst. and Methods in Physics Research, A

journal homepage: www.elsevier.com/locate/nima

Silicon carbide neutron detector testing at the JSI TRIGA reactor for enhanced border and port security

Vladimir Radulović [a,*], Yuichi Yamazaki [b], Željko Pastuović [c], Adam Sarbutt [c], Klemen Ambrožič [a], Robert Bernat [d], Zoran Ereš [d], José Coutinho [e], Takeshi Ohshima [b], Ivana Capan [d], Luka Snoj [a,f]

[a] Jožef Stefan Institute, Jamova cesta 39, SI-1000 Ljubljana, Slovenia
[b] National Institutes for Quantum and Radiological Science and Technology, 1233 Watanuki, Takasaki, Gunma 370-1292, Japan
[c] Australian Nuclear Science and Technology Organisation, 1 New Illawarra Rd., Lucas Heights, NSW 2234, Australia
[d] Rudjer Bošković Institute, Bijenička 54, 10000 Zagreb, Croatia
[e] Department of Physics and I3N, University of Aveiro, 3810-193 Aveiro, Portugal
[f] University of Ljubljana, Faculty of Mathematics and Physics, Jadranska cesta 19, 1000 Ljubljana, Slovenia

ARTICLE INFO

Keywords:
Silicon carbide
Neutron detection
Neutron converter
JSI TRIGA reactor

ABSTRACT

In 2016, the NATO Science for Peace and Security Programme funded research project "Engineering Silicon Carbide for Border and Port Security" — E-SiCure was launched, its objective being the development of radiation-hard silicon carbide (SiC) based detectors of special nuclear materials (SNM), with the aim to enhance border and port security barriers. Detector prototypes based on SiC Schottky Barrier Diodes (SBDs) and neutron converter films were developed. This paper presents the results of a dedicated experimental testing campaign performed at the Jožef Stefan Institute (JSI) TRIGA reactor in which several SiC detector prototypes equipped with ^{10}B and ^{6}LiF converter films were irradiated in the Dry Chamber of the reactor. The obtained results demonstrate a clearly measurable neutron response, which varies linearly with the neutron flux. The measured particle spectra from the SiC detectors exhibit a clear structure, attributable to the nature and energy of secondary particles originating as reaction products from nuclear reactions involving ^{10}B and ^{6}Li isotopes. The determined sensitivity of the detectors, their active volume being 1 mm × 1 mm × 25 μm, 1 mm × 1 mm × 69 μm and 1 mm × 1 mm × 170 μm, was of the order of 2×10^{-5} counts per second, per unit of neutron flux [counts s^{-1} per n $cm^{-2}s^{-1}$] (for neutron energies between 0 and 5 eV). Scaling the detection sensitivity by a factor of 10^5, i.e. to an array with a surface of around 20 cm × 2 m, comparable to large BF_3 or ^{3}He detectors, would theoretically enable an overall sensitivity of around 2 counts s^{-1} per n $cm^{-2}s^{-1}$, which is already comparable to typical neutron sensitivity values of gas detectors, in the range from several to over 100 counts s^{-1} per n $cm^{-2}s^{-1}$. Due to its outstanding tolerance to harsh environments (including high temperatures and radiation fields) and superior electronic properties when compared to other semiconductors, SiC is a promising base material for the fabrication of solid-state detectors with stable and long life-time. Improvements in sensitivity combined with the capability of fabricating large modules (SiC arrays), could make SiC an important detection technology, applicable also in the context of border and port security barrier monitoring.

1. Introduction

Increasingly complex risks like geopolitical instability or decentralized terrorism threats, have led to the urge for deploying nuclear screening systems for detection of illicit trafficking of nuclear materials, and consequently, to a growing interest in the field of research and development of new radiation detection technologies suitable for homeland security applications. Development of neutron-sensing detectors in the last two decades was driven by specific applications, shifting from niche (scientific research, fuel monitoring in nuclear power stations, enforcement of non-proliferation and arms-control treatises [1–3]) to public-wide applications, ranging from agriculture to homeland security [4,5]. Recent progress in the manufacturing of high-quality bulk and epitaxial silicon carbide (SiC) driven by a mature and growing industry of power electronics [6–8], could enable unprecedented opportunities for future SiC-based detection of neutron and alpha particle sources. Unlike existing and commonly used gas-based neutron detectors, SiC-based devices have the potential advantages of high

* Corresponding author.
E-mail address: vladimir.radulovic@ijs.si (V. Radulović).

https://doi.org/10.1016/j.nima.2020.164122
Received 11 September 2019; Received in revised form 29 April 2020; Accepted 7 May 2020
Available online 11 May 2020

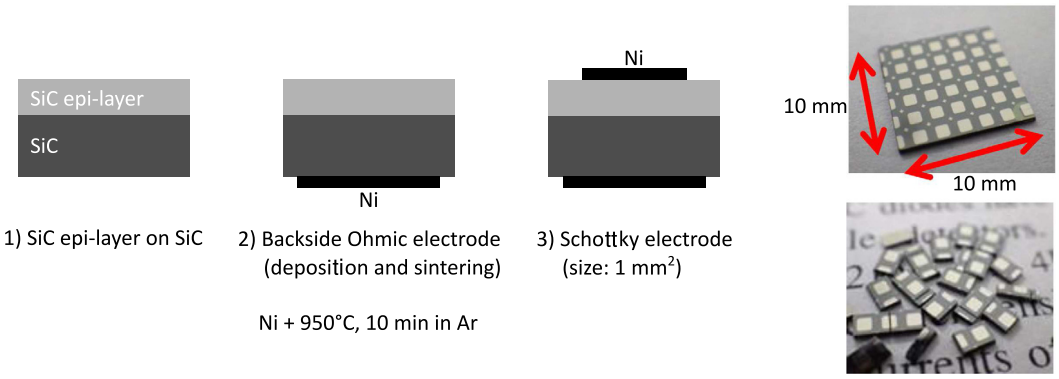

Fig. 1. Schematic display of the SiC SBD fabrication process.

production scalability, low operation voltage, portability, on-chip integration and pixelization, as well as good discrimination against gamma radiation. More importantly, due to its extreme radiation hardness, silicon carbide (more specifically its 4H hexagonal phase - 4H-SiC) [9,10], has been seen as a promising semiconductor to be used as the active volume for solid-state radiation and particle detectors, including X-rays [11], alpha-particles [12,13] and neutrons [14–18].

In 2016, the NATO Science for Peace and Security Programme funded research project "Engineering Silicon Carbide for Border and Port Security" - E-SiCure was launched, with the main objective of combining theoretical, experimental and applied research towards the development of radiation-hard SiC-based detectors of special nuclear materials (SNM), in order to enhance border and port security barriers. The initial project activities were devoted to studies of material radiation hardness and modification processes in order to manipulate the most severe electrically active defects which trap or annihilate free charge carriers, by specific ion implantation and defect engineering [19–21].

This paper presents the results of neutron detection testing activities performed at the Jožef Stefan Institute (JSI) TRIGA reactor in the framework of the E-SiCure project. Section 2 presents SiC Schottky Barrier Diode (SBD) detector prototypes and a data acquisition system developed within the E-SiCure project. It also presents the results from initial testing using an ^{241}Am alpha particle source. Section 3 describes the realization of SiC detector prototypes, including neutron converter films based on ^{10}B and ^{6}LiF. Section 3 also describes a series of tests using an ^{241}Am alpha particle source and the results of neutron irradiation testing in the JSI TRIGA reactor. Section 4 gives a discussion of the obtained results and outlines future areas of investigation.

2. SiC detector prototypes and data acquisition system

Several prototype neutron detectors were manufactured at the National Institutes for Quantum and Radiological Science and Technology in Japan (QST), specifically for experimental testing of alpha particle and neutron response. The detectors were based on n-type 4H-SiC SBDs with several active layer thicknesses and dopant concentrations (N_D): 25 μm ($N_D = 4.7\times10^{14}$ cm^{-3}), 69 μm ($N_D = 9.1\times10^{14}$ cm^{-3}) and 170 μm ($N_D = 4.8\times10^{14}$ cm^{-3}), their lateral dimensions being 1 mm × 1 mm. The diodes were fabricated by growth of a SiC epitaxial layer onto the SiC substrate and subsequent deposition and sintering of nickel Ohmic and Schottky contacts. The contact quality was verified with I-V and C-V measurements. The fabrication process of SiC SBDs is schematically displayed in Fig. 1.

The detectors consisted of SBDs, surface-mounted onto chip carriers with wire bonded electrical contacts, as displayed in Fig. 2. The chip carriers were enclosed in 3D-printed plastic holders in order to completely isolate the electrical contacts under high voltage. The holders were mounted in aluminium enclosures; the holders and aluminium

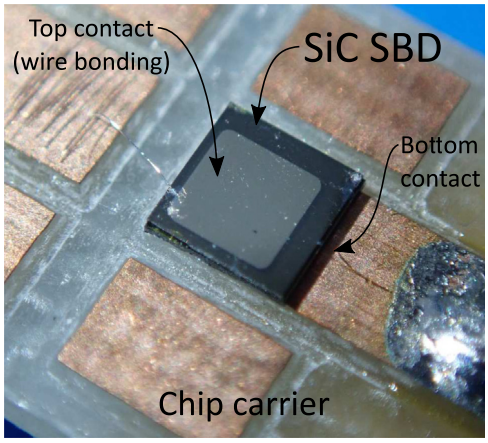

Fig. 2. Closeup of a SiC detector.

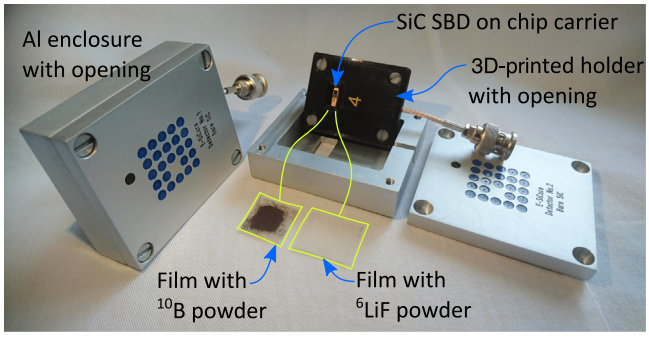

Fig. 3. Prototype detectors. Left: assembled detector prototype in aluminium enclosure. Right: prototype detector components: SiC SBD mounted onto chip carrier with contacts, installed in 3D printed holder with opening, converter films (with ^{10}B and ^{6}LiF powder), open aluminium enclosure with opening.

enclosures had an opening directly above the SBD to enable charged particles to reach the SBD surface, as displayed in Fig. 3.

The electronic system for particle event processing and recording consisted of a preamplifier and a shaping amplifier (PCB modules CR-150-R5 and CR-160-R7) manufactured by CREMAT, and a digital signal processing multichannel analyser (DSP-MCA) manufactured by AMPTEK (model no. 8000D), operated by a laptop computer. Fig. 4 displays a schematic diagram of the electronic data acquisition system.

Power to the electronic system (preamplifier and shaping amplifier) was provided by a standalone battery-powered voltage source, in order to avoid the use of mains power. The latter often carries electronic noise which can negatively affect the measurement performance. The voltage

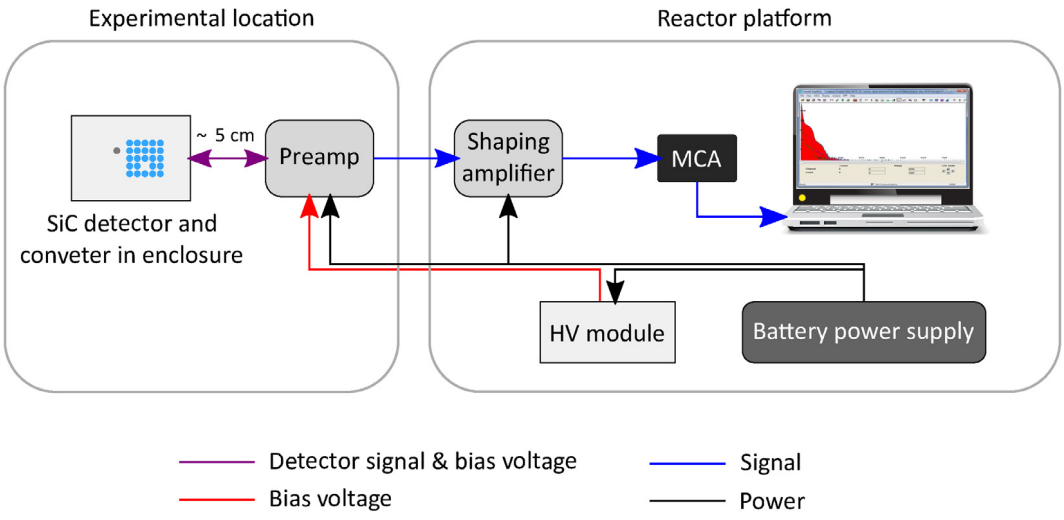

Fig. 4. Schematic diagram of the electronic data acquisition system.

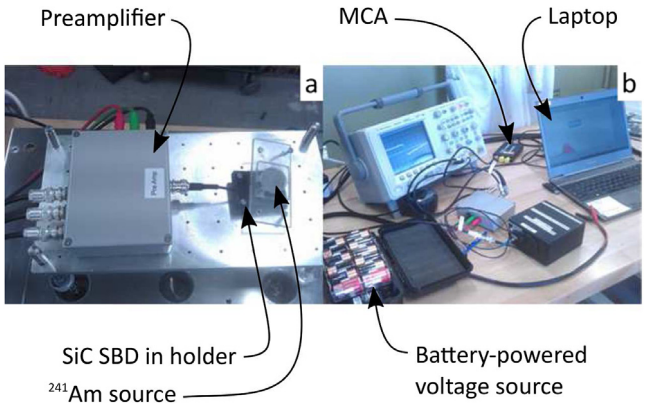

Fig. 5. Detector system under development: (a) A SBD detector being tested using a ^{241}Am source. (b) Electronic system for operation of a detector and data acquisition during initial testing at ANSTO.

source also provided power to a separate high voltage bias module, used to apply reverse bias to the SBDs. Reverse negative bias was connected to the front Schottky contact of the SBDs, the back Ohmic contact of the prepared prototype detectors was grounded.

Initial testing of the detectors and acquisition system was performed in low-AC-noise environment in the detector laboratory at the Australian Nuclear Science and Technology Organisation (ANSTO). The acquisition system was tested using a precision pulse generator. An ^{241}Am alpha particle source was used to test the detector response to energetic charged particles. The experimental setup for the initial testing is displayed in Fig. 5.

In order to keep a low capacitance input (10 pF) to the preamplifier stage, we used a CREMAT CR-110-R2 preamplifier chip and tested the detection energy resolution with the shaping PCB module equipped with a CR-200-R2 chip with shaping times of 0.5 and 1.0 μs. The total gain for event signal amplification was kept constant. Pole/Zero (P/Z) was adjusted for different shaping constants. Recorded events were sorted by the MCA in 2k-channel energy spectra. The performance of the detection system was observed for shaping times of 0.5 and 1.0 μs and reverse bias voltages of 50 and 100 V. The combination of a reverse bias voltage of 50 V and a shaping time of 1 μs resulted in best spectroscopic performance. The initial testing results demonstrated the functionality of the detector prototypes and the electronic measurement system.

3. Neutron detection testing

3.1. Neutron detector prototypes

Following the results obtained from the initial testing, an experimental campaign was performed at the JSI TRIGA reactor in May 2018 aiming at demonstrating and quantifying the neutron detection capabilities of the prototype detectors in terms of their neutron detection sensitivity. For the test, four new detectors were realized. The detector prototypes were equipped with converting films for thermal neutron detection. Due to the very large thermal neutron cross sections of the $^{10}B(n,\alpha)^{7}Li$ and $^{6}Li(n,t)^{4}He$ reactions (around 3843 b and 938 b respectively, at an incident neutron energy of 0.0253 eV [22]), and the production of detectable energetic charged particles, the chosen converting materials were enriched ^{10}B and ^{6}LiF powders. The ^{10}B and ^{6}LiF powders were applied onto plastic film and mounted above the openings of the 3D-printed SBD holders, at a distance of approximately 2 mm from the SBD surface. Fig. 3 shows two prototype detectors used in the experimental tests (fully enclosed and open).

3.2. ^{241}Am alpha particle testing

Firstly, the detectors were tested without neutron converters and no radiation sources, with an applied HV bias of 50 V. All the obtained spectra showed a large peak at low channel numbers, which was attributed to electronic noise, and no counts appeared at higher channels. The detectors were then tested using an ^{241}Am alpha source, its nominal activity being 416 kBq. Measurements were taken at two different times, in the first session using a 25 μm and a 170 μm detector, in the second using a 69 μm detector the same 170 μm detector as in the first session. In all the recorded spectra, a clear peak due to the alpha particles emitted from ^{241}Am at high channels was observed, confirming the functioning of the SBDs as detectors of charged particles. Fig. 6 displays the recorded ^{241}Am particle spectra. The ^{241}Am α peak (E = 5485.6 keV) appears in the range between channels 4500–4700. In Fig. 6, (1) and (2) indicate the first and second measurement of the ^{241}Am α particle spectrum using the 170 μm detector. The observed slight difference in the position of the ^{241}Am α particle peak (around 5%) between the detector spectra is attributable to several

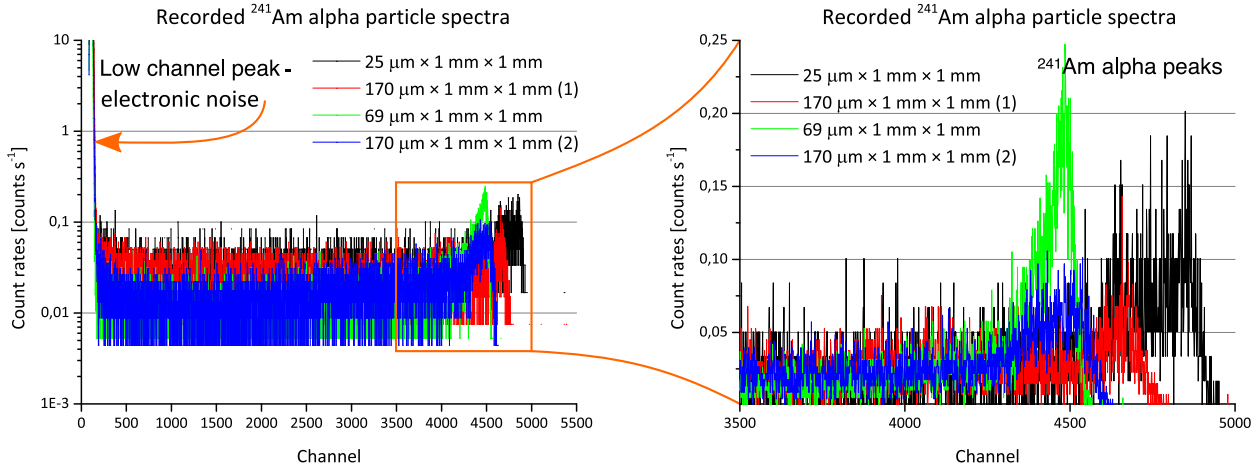

Fig. 6. Recorded ^{241}Am particle spectra.

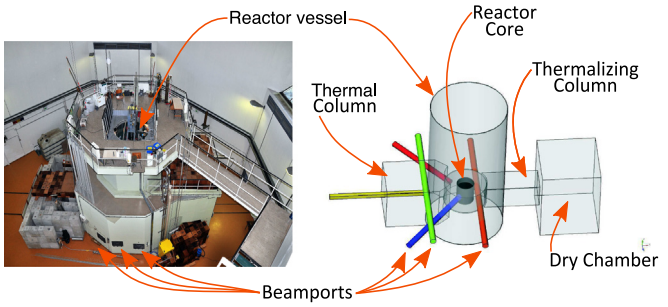

Fig. 7. Photograph and schematic view of the main components of the JSI TRIGA reactor.

Table 1
Neutron flux levels in the Dry Chamber of the JSI TRIGA reactor corresponding to the power levels at which the prototype SiC detectors were irradiated. ϕ_{tot} are the total flux values, $\phi_{0-5\ eV}$ are the flux values in the range from 0 to 5 eV, relevant for the ^{10}B(n,α) and ^{6}Li(n,t) nuclear reactions (Section 3.5).

P [kW]	ϕ_{tot} [n cm^{-2}s^{-1}]	$\phi_{0-5\,eV}$ [n cm^{-2}s^{-1}]
0	0	0
10	6.4×10^{5}	3.5×10^{5}
50	3.2×10^{6}	1.8×10^{6}
100	6.4×10^{6}	3.5×10^{6}
170	1.1×10^{7}	6.0×10^{6}
180	1.2×10^{7}	6.3×10^{6}
250	1.6×10^{7}	8.8×10^{6}

possible causes, e.g. temporal drifts in the acquisition system parameters, polarization effects due e.g. to differences in the quality of the electrical contacts, and differences in the source-to-detector distance during these measurements (estimated at 5 mm ± 2 mm). It is worth noting that these measurements were performed essentially as a means of verification of the functioning of the detectors and acquisition system before irradiation with neutrons; each irradiation involving a rather time-consuming manipulation procedure.

3.3. Neutron irradiation testing

Following the α particle tests, the neutron converter films were applied to the detectors and neutron irradiations were performed in the Dry Chamber of the JSI TRIGA reactor. The Dry Chamber is a large irradiation room in the concrete body of the reactor, connected with the reactor core by a graphite thermalizing column [23]. It is mostly used for radiation hardness testing of detectors, electronic components and systems [24,25]. Fig. 7 displays a photograph of the JSI TRIGA reactor and a schematic view of its main components, including the Dry Chamber.

Measurements were taken firstly with 25 μm and 170 μm thick detector prototypes, both equipped with ^{10}B converter films at the following reactor power levels: 10 kW, 50 kW, 100 kW, 180 kW and 250 kW. The determination of the corresponding neutron flux levels is discussed in Section 3.5; Table 1 reports the neutron flux levels corresponding to each power level the detectors were irradiated at. In all the recorded spectra we observed a significant number of counts at higher energy channels. We also observed a distinctive structure, which was similar in all the recorded spectra.

Measurements were continued with 69 μm and 170 μm thick detector prototypes equipped with ^{6}LiF and ^{10}B converter films, respectively (the latter film was prepared using a smaller quantity of ^{10}B powder), at the following reactor power levels: 10 kW, 50 kW, 100 kW, 170 kW and 250 kW. As for the ^{10}B converter film, with the ^{6}LiF converter film we also observed a significant number of counts at higher energy channels. In the measured spectra obtained with the 69 μm detector prototype equipped with the ^{6}LiF converter film, we also observed a distinctive structure in all the spectra, which was qualitatively different to the one observed using ^{10}B converter film.

The energy calibration (relation between energy and channel number) for the recorded spectra was obtained from the measurements of ^{241}Am alpha peaks only. Measurements were performed with other alpha particle sources (^{230}Th and ^{232}Th), however their activities were not sufficiently high to be able to obtain usable particle spectra. Therefore a linear relationship was assumed with intercept at zero. Figs. 8 and 9 display the measured spectra in which the structure was the clearest, obtained with a 25 μm × 1 mm × 1 mm SiC SBD, equipped with a ^{10}B converter film and a 69 μm × 1 mm × 1 mm SiC SBD, equipped with a ^{6}LiF converter film, respectively, with the energy calibrations applied.

3.4. Interpretation of the measured spectra

The reactions used for the conversion of neutrons to charged particles are ^{10}B(n,α) and ^{6}Li(n,t). The ^{10}B(n,α) reaction can take place through two reaction channels:

$$^{10}\mathrm{B} + n \rightarrow \alpha(1776\ \mathrm{keV}) + {}^{7}\mathrm{Li}\ (1013\ \mathrm{keV});\ \mathrm{BR} = 6.3\%;\ Q = 2789.5\ \mathrm{keV}$$

$$^{10}\mathrm{B} + n \rightarrow \alpha(1472\ \mathrm{keV}) + {}^{7}\mathrm{Li}^{*}\ (840\ \mathrm{keV});\ \mathrm{BR} = 93.7\%;\ Q = 2311.9\ \mathrm{keV},$$

where ^{7}Li* represents an excited state of ^{7}Li, BR denotes the branching ratio and Q the reaction Q value. The measured spectra using the 25 μm × 1 mm × 1 mm SiC SBD, equipped with a ^{10}B converter layer

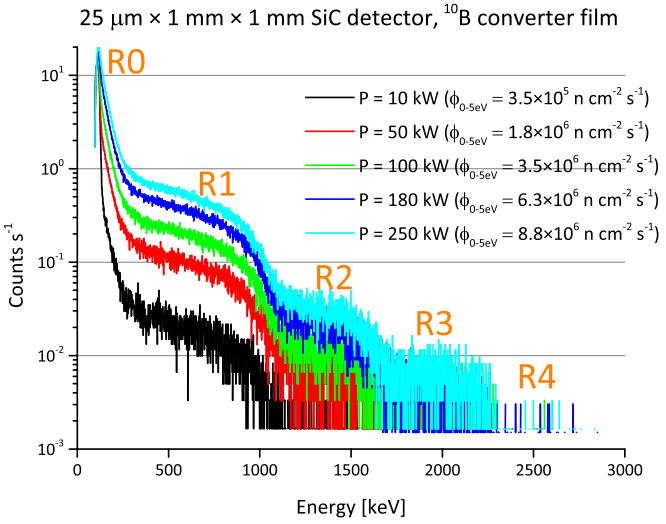

Fig. 8. Spectra from 25 μm with ^{10}B converter layer.

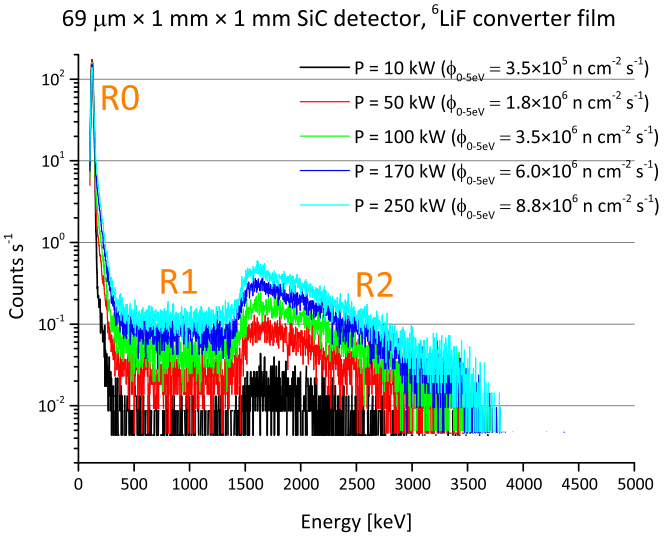

Fig. 9. Spectra from 69 μm with ^{6}LiF converter layer.

(Fig. 8) display a distinctive structure, attributable to the secondary charged particles originating from $^{10}B(n,\alpha)$ reactions. The main features (regions) in the spectra are denoted with "R0" - "R4". Table 2 gives the energy ranges of the observed regions and possible interpretations of the detected events.

The $^6Li(n,t)$ reaction takes place through one reaction channel:

$$^6Li + n \rightarrow t(2731\ \text{keV}) + \alpha(2052\ \text{keV}); Q = 4783\ \text{keV}$$

In the case of the spectra obtained using the ^{6}LiF converter layer the interpretation is not straightforward. The broad regions observed in the spectra are denoted with "R0" - "R2". Table 3 gives the energy ranges of the observed regions and possible interpretations of the detected events. The observed low spectroscopic performance of the detectors equipped with ^{6}LiF converters is probably due to the low intrinsic energy resolution of the detectors and partial slowing down of the charged particles in the converter layers themselves. As a comparison, significantly better energy resolution is achievable with diamond detectors and thin ^{6}LiF converter layers [26].

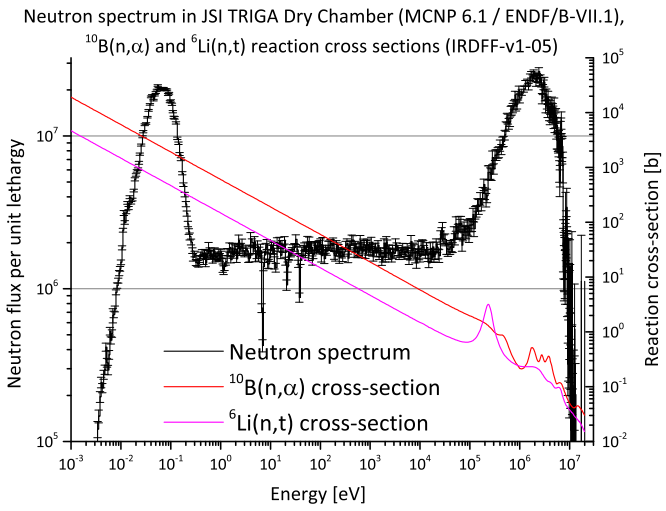

Fig. 10. Neutron spectrum in the Dry Chamber of the JSI TRIGA reactor obtained with a Monte Carlo particle transport calculation with the MCNP6.1 code/ENDF/B-VII.1 nuclear data library.

3.5. Neutron flux determination through activation measurements

In order to determine the order of magnitude of the neutron sensitivity of the prototype detectors, activation dosimetry measurements for the $^{197}Au(n,\gamma)^{198}Au$ reaction were carried out in the Dry Chamber of the JSI TRIGA reactor in the location used for the measurements with SiC detectors. The measured $^{197}Au(n,\gamma)^{198}Au$ reaction rate was $7.4(1 \pm 0.03) \times 10^{-16}$ s^{-1} per target atom. The total neutron flux level was determined on the basis of the measured reaction rate, and the neutron spectrum in the irradiation location in the Dry Chamber, obtained from a Monte Carlo particle transport calculations with the MCNP6.1 code [27] in conjunction with the ENDF/B-VII.1 nuclear data library [28], using a detailed, verified and validated computational model of the JSI TRIGA reactor [29–33].

Fig. 10 displays the calculated neutron spectrum in the Dry Chamber of the JSI TRIGA reactor, along with the $^{10}B(n,\alpha)$ and $^6Li(n,t)$ reaction cross-sections. The total neutron flux level was determined assuming the calculated neutron spectrum shape, and normalizing the total neutron flux level to reproduce the experimental $^{197}Au(n,\gamma)^{198}Au$ reaction rate value. The determined total neutron flux at full reactor power at the position in which the prototype neutron detectors were tested was 1.6×10^7 n cm^{-2} s^{-1}. The neutron flux is linearly proportional to the reactor power.

The $^{10}B(n,\alpha)$ and $^6Li(n,t)$ reactions both have $1/v$ dependent cross-sections practically up to the fission neutron energy range, and are therefore predominantly sensitive to thermal neutrons. Therefore, for the determination of the neutron detection sensitivity, instead of the total neutron flux, it is physically more appropriate to consider only the neutron energy range which gives rise to the majority of the detected signal. In the present work, we consider $E = 0$ as the bottom energy limit and $E = E_{99\%}$ (i.e. the energy at which the cumulative reaction rates reaches 99% of its total values) as the top energy limit.

Fig. 11 displays the cumulative reaction rates for the $^{10}B(n,\alpha)$, $^6Li(n,t)$ and $^{197}Au(n,\gamma)$ reactions, computed using the JSI developed code RR_UNC, which calculates reaction rates and their uncertainties due to uncertainties in the reaction cross-sections and neutron spectra [34]. The cumulative reaction rates were computed with the neutron spectrum in the Dry Chamber (Fig. 10) and cross-sections from the IRDFF-v1-05 dosimetry nuclear data library. The cumulative reaction rates are normalized to the total reaction rate values. Along with the cumulative reaction rate curves, the $E_{99\%}$ values are also denoted. For both $^{10}B(n,\alpha)$ and $^6Li(n,t)$, the calculated $E_{99\%}$ values are between 4 and 5 eV, therefore, for the sake of consistency, $E = 5$ eV was set as the top energy limit.

Table 2
Features in the measured spectra using a 25 μm ×1 mm ×1 mm SiC SBD, equipped with a ^{10}B converter layer.

Region	Energy range, approx. [keV]	Detected events
R0	0–300	Electronic noise and γ background
R1	300–1100	^{7}Li and ^{7}Li* particles (E = 839.8 keV, E = 1013, 3 keV)
R2	1100–1700	α particles (E = 1472.1 keV, E = 1776.2 keV)
R3	1700–2300	α particles (E = 1472.1 keV) and ^{7}Li* particles (E = 839.8 keV) from dominant reaction channel detected simultaneously
R4	2300–2700	α particles (E = 1776.2 keV) and ^{7}Li particles (E = 1013.3 keV) from less probable reaction channel detected simultaneously

Table 3
Features in the measured spectra using a 69 μm ×1 mm ×1 mm SiC SBD, equipped with a ^{6}LiF converter layer.

Region	Energy range, approx. [keV]	Detected events
R0	0–300	Electronic noise and γ background
R1	300–1400	Partial energy deposition events
R2	1400–3800	Partial energy deposition from t (E = 2731 keV) and α (E = 2052 keV) particles

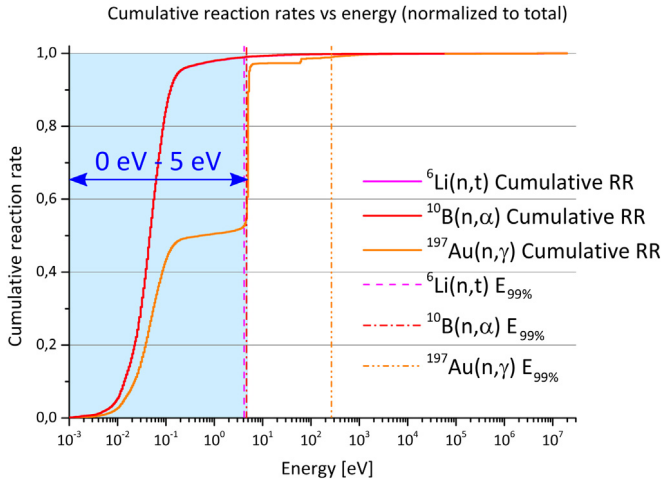

Fig. 11. Cumulative reaction rates for the $^{10}B(n,\alpha)$, $^{6}Li(n,t)$ and $^{197}Au(n,\gamma)$ reactions. The vertical lines denote the energies at which the cumulative reaction rates reach 99% of their total values. The $^{10}B(n,\alpha)$ $^{6}Li(n,t)$ reactions are sensitive to the neutron energy region between 0 and 5 eV, highlighted in blue. (For interpretation of the references to colour in this figure legend, the reader is referred to the web version of this article.)

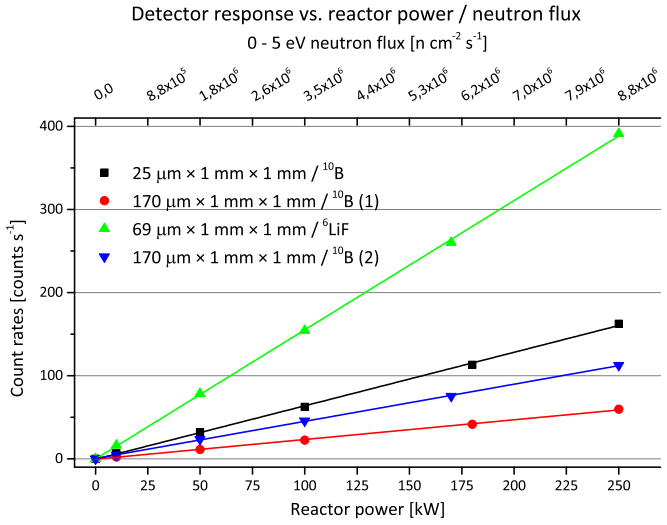

Fig. 12. Total detected count rates (above channel no. 500), i.e. around 600 keV as a function of reactor power/neutron flux. The lines represent fitted linear relationships to the data.

3.6. Detector response vs. neutron flux

Two very important parameters of a neutron detector are the detection sensitivity and response linearity. In practical applications of SiC neutron detectors, it is reasonable to assume that the total neutron signal is derived from the total detector count rates above a certain energy threshold, applied to suppress the contribution due to electronic noise. Furthermore, semiconductor detectors are expected to be combined into arrays to increase the overall detection sensitivity. On the basis of the measured particle spectra obtained during the testing campaign at the JSI TRIGA reactor, we applied a threshold at channel no. 500 (corresponding to the incident energy of around 600 keV), which is definitely above the low energy peak, attributed to electronic noise. Fig. 12 displays the total detected count rates as a function of reactor power and corresponding neutron flux. The graphs in Fig. 12 demonstrate excellent response linearity.

The detection sensitivity per unit of neutron flux is represented by the slope in the graphs in Fig. 12. The computed values for the tested detectors are reported in Table 4. The neutron flux between 0 and 5 eV was considered.

In view of the end application, in which SiC detectors would be employed as monitors in the context of border and port security, it is

Table 4
Computed detector sensitivities from this work, scaled sensitivity and typical sensitivities for BF_3 and ^{3}He detectors.

Detector/Converter	Sensitivity [counts s^{-1} per n cm^{-2} s^{-1}]
25 μm × 1 mm × 1 mm/^{10}B	1.8×10^{-5}
170 μm × 1 mm × 1 mm (1)/^{10}B	6.4×10^{-6}
69 μm × 1 mm × 1 mm/^{6}LiF	4.4×10^{-5}
170 μm × 1 mm × 1 mm (2)/^{10}B	1.3×10^{-5}
Scaled sensitivity to 100 × 1000 array of SiC detectors	around 2
Typical BF_3	around 4
Typical ^{3}He	several 10 - above 100

envisaged that a large number of detectors would be configured into arrays. Typical dimensions of BF_3 or ^{3}He neutron monitor detectors used in this application are 2.54 cm – 5.08 cm (1 inch – 2 inches) in diameter and 0.3 m – 1.8 m in length. Typical sensitivity values for BF_3 detectors are of the order of 4 counts s^{-1} per n $cm^{-2}s^{-1}$, for ^{3}He detectors in the range of several 10 to over 100 counts s^{-1} per n $cm^{-2}s^{-1}$. Assuming a uniform neutron field, an array of 100 × 1000 SiC detectors with a neutron sensitivity of 2×10^{-5} counts s^{-1} per n $cm^{-2}s^{-1}$ for each single detector (as demonstrated in this work), with dimensions comparable to large ^{3}He neutron monitors (around 0.2 m × 2 m), would theoretically allow an overall sensitivity of around 2 counts s^{-1} per n $cm^{-2}s^{-1}$, which is already comparable to typical neutron sensitivity values offered by gas detectors currently available on the market.

However, for detectors used in the context of border and port security, there is a strong interest to decrease their complexity and thereby the associated manufacturing and maintenance cost, while increasing robustness and ease of operation. The obvious way forward is development work aimed at reducing the required number of single SiC detectors, as each one requires a separate electronic data acquisition line, by increasing the sensitivity of single SiC detectors.

There are several important factors influencing the sensitivity of a SiC-based neutron detector. To some extent, SBDs with a larger active area would allow a larger neutron count rate, by enabling a larger fraction of the charged particles emitted from the converter film to be detected. However, the maximum size of the SBDs is limited by degradation of the electronic properties due to the manufacturing process and the overall capacitance, which negatively affects their charged particle detection performance. In the detector prototypes in the present work, an air gap exists between the neutron converter film and the SiC SBDs, which partially slows down the emitted charged particles. Placing the SiC SBDs and the neutron converter film in an evacuated environment (as is implemented in α spectrometry devices) would reduce the dissipation of the kinetic energy of the emitted charged particles, and therefore improve the detection performance. Lastly, the thickness of the neutron converter film strongly affects the self-absorption of the charged particles. An optimal converter thickness enables maximizing the reaction rate and the kinetic energy of the charged particles escaping from the converter material. For this purpose, thin films of the order of 1 μm [35] are the most effective.

4. Conclusions and future work

This paper presents the development and testing of SiC SBD neutron detector prototypes and acquisition systems performed in the NATO SPS-funded project E-SiCure, with the motivation to pave the way for the application of SiC detector technology for enhanced border and port security barriers.

It is demonstrated that simple detection devices based on SiC SBDs, equipped with neutron to charged particle converter films, based on ^{10}B and ^{6}Li isotopes, have a clearly measurable neutron response, which varies linearly with the incident neutron flux. Furthermore, extrapolating the experimental neutron sensitivity values of single SiC SBDs to larger arrays of such detectors, theoretically, a response comparable to neutron detectors currently in use for this application is achievable. However, at the present neutron detection sensitivity, very large detector arrays would be required, implying a high degree of system complexity and serious technical challenges related to the implementation and operation, and a high cost.

For detector applications in the context of border and port security, there is a strong interest in reducing the number of single SiC detectors, which could be made possible by increasing the performance of single SiC diodes. Further development work is required, aimed at increasing the sensitivity of single SiC detectors, and, more importantly, at solving the technical challenges associated to the construction and signal readout from a large array of single SiC devices.

CRediT authorship contribution statement

Vladimir Radulović: Investigation, Writing - original draft, Writing - review & editing. **Yuichi Yamazaki:** Resources. **Željko Pastuović:** Investigation, Supervision. **Adam Sarbutt:** Resources. **Klemen Ambrožič:** Formal analysis. **Robert Bernat:** Investigation. **Zoran Ereš:** Validation. **José Coutinho:** Formal analysis, Supervision. **Takeshi Ohshima:** Methodology, Supervision. **Ivana Capan:** Project administration, Conceptualization, Funding acquisition, Supervision. **Luka Snoj:** Project administration, Supervision.

Declaration of competing interest

The authors declare that they have no known competing financial interests or personal relationships that could have appeared to influence the work reported in this paper.

Acknowledgements

The present work was financially supported by the NATO Science for Peace and Security Programme, Belgium, under project no. SPS 985215 - Engineering Silicon Carbide for Border and Port Security — E-SiCure. The JSI project team would like to acknowledge the support from the Slovenian Ministry of Education, Science and Sport (project no. P2-0073 - Reactor Physics). The RBI project team would like to acknowledge financial support from the European Regional Development Fund for the "Center of Excellence for Advanced Materials and Sensing Devices" (Grant No. KK.01.1.1.01.0001). JC acknowledges the Fundação para a Ciência e a Tecnologia (FCT), Portugal through project UID/CTM/50025/2013.

References

[1] S. Fetter, et al., Detecting nuclear warheads, Sci. Glob. Secur. 1 (3–4) (1990) 225–253.
[2] A. Glaser, B. Barak, R.J. Goldston, A zero-knowledge protocol for nuclear warhead verification, Nature 510 (2014) 497–502.
[3] S. Park, et al., Development of SiC detector for the harsh environment applications, in: 2013 IEEE Nuclear Science Symposium and Medical Imaging Conference, 2013 NSS/MIC, Seoul, 2013, pp. 1–4.
[4] R.T. Kouzes, et al., Neutron detection alternatives to 3He for national security applications, Nucl. Instrum. Methods A 623 (3) (2010) 1035–1045.
[5] A. Wahbi, L. Heng, G. Dercon, Cosmic Ray Neutron Sensing: Estimation of Agricultural Crop Biomass Water Equivalent, Springer, 2018.
[6] T. Kimoto, Material science and device physics in SiC technology for high-voltage power devices, Japan. J. Appl. Phys. 54 (2015) 040103.
[7] X. She, et al., Review of silicon carbide power devices and their applications, IEEE Trans. Ind. Electron. 64 (10) (2017) 8193–8205.
[8] J. Wang, et al., IEEE ITRW working group position paper-system integration and application: Silicon carbide: A roadmap for silicon carbide adoption in power conversion applications, IEEE Power Electron. Mag. 5 (2) (2018) 40–44.

[9] W.J. Choyke, H. Matsunami, G. Pensl, Silicon Carbide, Springer, 2004.
[10] T. Kimoto J. A. Cooper, Fundamentals of Silicon Carbide Technology: Growth, Characterization, Devices, and Applications, Singapore, John Wiley & Sons, 2014.
[11] G. Lioliou, et al., 4H-SiC Schottky diode arrays for X-ray detection, Nucl. Instrum. Methods A. 840 (2016) 145–152.
[12] F. Nava, et al., Minimum ionizing and alpha particles detectors based on epitaxial semiconductor silicon carbide, IEEE Trans. Nucl. Sci. 51 (1) (2004) 238–244.
[13] F.H. Ruddy, et al., High-resolution alpha-particle spectrometry using silicon carbide semiconductor detectors, in: IEEE Nuclear Science Symposium Conference Record, 2005, Fajardo, 2005, pp. 1231–1235.
[14] A.R. Dulloo, The thermal neutron response of miniature silicon carbide semiconductor detectors, Nucl. Instrum. Methods A 498 (1–3) (2003) 415–423.
[15] F. Franceschini, F.H. Ruddy, Silicon carbide neutron detectors, in: Rosario Gerhardt (Ed.), Properties and Applications of Silicon Carbide, InTech, Rijeka, 2011 (Chapter 13).
[16] F. Issa, et al., Radiation silicon carbide detectors based on ion implantation of boron, IEEE Trans. Nucl. Sci. 61 (2014) 2105–2111.
[17] D. Szalkai, et al., Fast neutron detection with 4H-SiC based diode detector up to 500C ambient temperature, IEEE Trans. Nucl. Sci. 63 (2016) 1491–1498.
[18] O. Obraztsova, et al., Comparison between silicon-carbide and diamond for thermal neutron detection at room temperature, in: ANIMMA 2017 – Advancements in Nuclear Instrumentation Measurement Methods and their Applications, EPJ Web Conf., Vol. 170, 2018.
[19] I. Capan, et al., Double negatively charged carbon vacancy at the h- and k- sites in 4H-SiC: Combined Laplace-DLTS and DFT study, J. Appl. Phys. 123 (2018) 161597.
[20] I. Capan, et al., Deep level defects in 4H-SiC epitaxial layers, Mater. Sci. Forum 924 (2018) 225–228.
[21] T. Brodar, et al., Laplace DLTS study of deep defects created in neutron-irradiated n-type 4H-SiC, Nucl. Instrum. Methods Phys. Res. B 437 (2018) 27–31.
[22] R. Capote, et al., Updating and extending the IRDF-2002 dosimetry library, J. ASTM Int. 9 (4) (2012) 1–9.
[23] V. Radulović, et al., Characterization of ex-core irradiation facilities of the JSI TRIGA Mark II reactor, in: Proceedings, 21st International Conference Nuclear Energy for New Europe, September 5–7, Ljubljana, Slovenia, 2012.
[24] I. Mandić, et al., Bulk damage in DMILL npn bipolar transistors caused by thermal neutrons versus protons and fast neutrons, IEEE Trans. Nucl. Sci. 51 (4) (2004) 1752–1758.
[25] I. Mandić, V. Cindro, A. Gorišek, G. Kramberger, M. Mikuz, Online integrating radiation monitoring system for the ATLAS detector at the large hadron collider, IEEE Trans. Nucl. Sci. 54 (4) (2007) 1143–1150.
[26] S. Almaviva, et al., Thermal and fast neutron detection in chemical vapor deposition single-crystal diamond detectors, J. Appl. Phys. 103 (5) (2008) 054501.
[27] J.T. Goorley, M.R. James, T.E. Booth, F.B. Brown, J.S. Bull, L.J. Cox, J.W.J. Durkee, J.S. Elson, M.L. Fensin, R.A.I. Forster, et al., Initial MCNP6 Release Overview - MCNP6 Version 1.0, Report number: LANL Report LA-UR-13-22934, Los Alamos National Laboratory, 2013, June.
[28] M.B. Chadwick, et al., ENDF/B-VII.1 Nuclear data for science and technology: Cross sections, covariances, fission product yields and decay data, Nucl. Data Sheets 112 (12) (2011) 2887–2996.
[29] R. Jeraj, M. Ravnik, TRIGA mark II reactor: U(20)-zirconium hydride fuel rods in water with graphite reflector, IEU-COMP-THERM-003, in: International Handbook of Evaluated Criticality Safety Benchmark Experiments, NEA/NSC/DOC(95)03, OECD-NEA, Paris, France, 2010.
[30] International Handbook of Evaluated Critical Safety Benchmark Experiments, Organization for Economic Cooperation and Development, Nuclear Energy Agency, NEA/NSC/DOC(95)03, Paris, published on DVD.
[31] L. Snoj, et al., Calculation of kinetic parameters for mixed TRIGA cores with Monte Carlo, Ann. Nucl. Energy 37 (2) (2010) 223–229.
[32] L. Snoj, et al., Analysis of neutron flux distribution for the validation of computational methods for the optimization of research reactor utilization, Appl. Radiat. Isot. 69 (1) (2011) 136–141.
[33] V. Radulović, et al., Validation of absolute axial neutron flux distribution calculations with MCNP with ^{197}Au(n, γ)^{198}Au reaction rate distribution measurements at the JSI TRIGA Mark II reactor, Appl. Radiat. Isot. 84 (2014) 57–65.
[34] A. Trkov, Private communication, Code availale at: https://www-nds.iaea.org/IRDFF/.
[35] G. Nowak, et al., Boron carbide coatings for neutron detection probed by x-rays, ions, and neutrons to determine thin film quality, J. Appl. Phys. 117 (3) (2015) 034901.